Journal of Structural Biology 196 (2016) 155–163

Contents lists available at ScienceDirect

Journal of Structural Biology

journal homepage: www.elsevier.com/locate/yjsbi

Biomineralization pathways in a foraminifer revealed using a novel correlative cryo-fluorescence–SEM–EDS technique

Gal Mor Khalifa [a], David Kirchenbuechler [b], Naama Koifman [c], Olga Kleinerman [c], Yeshayahu Talmon [c], Michael Elbaum [b], Lia Addadi [a], Steve Weiner [a,*], Jonathan Erez [d]

[a] Department of Structural Biology, Weizmann Institute of Science, 234 Herzl Street, Rehovot 7610001, Israel
[b] Department of Materials and Interfaces, Weizmann Institute of Science, 234 Herzl Street, Rehovot 7610001, Israel
[c] Department of Chemical Engineering and the Russell Berrie Nanotechnology Institute (RBNI), Technion-Israel Institute of Technology, Haifa 3200003, Israel
[d] Institute of Earth Sciences, The Hebrew University of Jerusalem, Jerusalem 91904, Israel

ARTICLE INFO

Article history:
Received 14 December 2015
Received in revised form 28 January 2016
Accepted 29 January 2016
Available online 30 January 2016

Keywords:
Biomineralization pathways
Foraminifera
Shell formation
Magnesium
Correlative microscopy

ABSTRACT

Foraminifera are marine protozoans that are widespread in oceans throughout the world. Understanding biomineralization pathways in foraminifera is particularly important because their calcitic shells are major components of global calcium carbonate production. We introduce here a novel correlative approach combining cryo-SEM, cryo-fluorescence imaging and cryo-EDS. This approach is applied to the study of ion transport processes in the benthic foraminifer genus *Amphistegina*. We confirm the presence of large sea water vacuoles previously identified in intact and partially decalcified *Amphistegina lobifera* specimens. We observed relatively small vesicles that were labelled strongly with calcein, and also identified magnesium (Mg)-rich mineral particles in the cytoplasm, as well as in the large sea water vacuoles. The combination of cryo-microscopy with elemental microanalysis and fluorescence imaging reveals new aspects of the biomineralization pathway in foraminifera which are, to date, unique in the world of biomineralization. This approach is equally applicable to the study of biomineralization pathways in other organisms.

1. Introduction

Mineral formation in biology involves the uptake of ions from the environment and/or from food, followed by their transport in both dissolved and solid forms to the final site of deposition usually in a mineralized tissue. The challenge is therefore to follow the pathways of both the anions and the cations from uptake until final deposition. Here we report a novel correlative approach to investigate aspects of biomineralization pathways, and apply it to the study of the biomineralization pathways in benthic foraminifera. We use the membrane impermeable dye calcein and energy dispersive X-ray spectroscopy (EDS) to provide information on elemental distributions within the complex cellular milieu revealed by cryo-SEM inside the cytosol.

Foraminifera are unicellular marine protozoans that produce mainly calcitic shells (Lee and Anderson, 1991). Foraminifera are widespread in oceans throughout the world (Hemleben et al., 1989; Murray, 1991), and are major contributors to calcium carbonate global production (Erez, 2003). Their shells accumulate on the ocean floor and are eventually fossilized into chalks and limestones. The chemical and stable isotopic compositions of their calcitic shells are used to reconstruct past ocean conditions (Broecker and Peng, 1982; Emiliani, 1955; Katz et al., 2010; Wefer et al., 1999). Relatively little is known, however, about the mechanisms by which foraminifera produce their shells. This information is necessary not only for understanding a widespread biomineralization process, but also for understanding the connections between shell chemistry and environmental parameters used for paleoclimate reconstruction (Erez, 2003).

Foraminifera form their shells by the addition of consecutive chambers. The chambers are interconnected and the cytoplasm streams between them (Cushman, 1947). Shell mineralization in foraminifera is, therefore, not a continuous process but occurs in pulses each time a successive chamber is added to the shell. The calcitic radial (also known as perforated) foraminifera form their new chambers by first producing an organic template (anlage) and further mineralizing it with calcite crystals from both the inner and outer sides of a thin organic matrix often called the primary organic sheet (Hottinger, 1986). Every time a new chamber is

* Corresponding author.
E-mail address: Steve.weiner@weizmann.ac.il (S. Weiner).

http://dx.doi.org/10.1016/j.jsb.2016.01.015
1047-8477/

formed, the foraminifer adds an additional shell layer to its entire outer surface in a process termed lamination (Hottinger, 1986) (Fig. 1, Movie in SI1). In addition it adds an internal layer of calcium carbonate called the inner lining (Hansen and Reiss, 1971).

Studies of various benthic foraminifera have shown that a major mode of ion uptake is via the incorporation (endocytosis) of sea water into vacuoles that enter into the cytoplasm (Bentov et al., 2009; Erez, 2003). These vacuoles provide the ions to the fluid that is in intimate contact with the site of mineralization and is most likely the source of calcium and most of the carbonate (Bentov et al., 2009; Erez, 2003).

Some perforated foraminifera store the calcium (Ca^{2+}) and inorganic carbon extracted from the sea water during the intervals between chamber construction (Anderson and Faber, 1984; Angell, 1979; Erez, 2003; Lea et al., 1995; Nehrke et al., 2013; ter Kuile and Erez, 1987, 1988; ter Kuile et al., 1989; Toyofuku et al., 2008). The fraction of ions destined for mineralization and derived from the intracellular Ca^{2+} pools varies between different species. Some species have no internal pools, some have small pools (Angell, 1979; Lea et al., 1995; Nehrke et al., 2013), and some have large pools which store significant amounts (up to 90%) of the Ca^{2+} needed for shell mineralization (Anderson and Faber, 1984; Erez, 2003; Toyofuku et al., 2008). The calculated concentrations of Ca^{2+} and carbonate in the intracellular pools suggest that these ions may be stored in the cytoplasm, possibly as an amorphous calcium carbonate (ACC) phase (Bentov et al., 2009; Erez, 2003), but no such mineral phase has been identified to date. Other studies obtained during proxy calibration experiments and based on shell chemistry are interpreted to suggest that Ca^{2+} and carbonate are stored in separate pools in the cytoplasm (Duenas-Bohorquez et al., 2011; Raitzsch et al., 2010). It has also been proposed that part of the Ca^{2+} ions are transported by Ca^{2+} pumps directly from sea water, with no lag time between incorporation into the cytoplasm and deposition in the shell wall, and/or part of the ions are transferred by sea water vacuolization (Mewes et al., 2015; Nehrke et al., 2013). Differences between various proposed biomineralization mechanisms may be attributed to different species being used in the studies. Clearly much remains to be understood about the biomineralization pathways.

The cellular environment of intact foraminifera cannot be well characterized by conventional optical imaging techniques due to scattering of light from the shell, which blurs the images of deeper levels. Observation by Cryo Scanning Electron Microscopy (cryo-SEM) of vitrified, freeze fractured biological samples allows access to the morphology of the internal environment at high resolution without requiring any modification of the specimen composition. However, the micrographs alone cannot distinguish the ion and mineral fluxes that underlie the biomineralization process. This information is provided by cryo energy-dispersive X-ray spectroscopy (EDS) of X-rays emitted from the specimen for local elemental identification, and by fluorescence imaging of calcein, a cell impermeable fluorescent dye that labels endocytosed seawater vacuoles and vesicles, binding to calcium ions. Images from the same sample in the same location are merged in a correlative manner using native landmarks, primarily the foraminifera shell and photosynthetic symbiont organisms. Use of vitrified materials across the analysis preserves in place any highly unstable phases, or even ions in solution. Imaging and analysis are therefore carried out on vitrified specimens.

We apply this approach to the study of aspects of the biomineralization ion pathway from sea water to the shell in the benthic symbiont-bearing foraminifera *Amphistegina lobifera* and *Amphistegina lessoni*. *Amphistegina* belongs to the calcitic radial-perforated foraminifera group. *A. lobifera* deposits a calcitic shell with a Mg^{2+} content of 4–5 mol% (Bentov and Erez, 2006). In this species, a new chamber is formed once every 1–2 days in the juvenile life stage (0–30 days old), and roughly once every 1–2 weeks during the adult life stage (Erez, 2003). Adult *A. lobifera* possess the largest cytoplasmic Ca^{2+} pool documented to date, storing up to 90% of the Ca^{2+} used for mineralization of a new chamber, whereas internal Ca^{2+} reservoirs are small in the juveniles (Erez, 2003; ter Kuile and Erez, 1987,1988; ter Kuile et al., 1989). Sea water endocytosis plays an important role in the biomineralization pathway of *A. lobifera* (Bentov et al., 2009). This incorporation process was demonstrated using in vivo labeling with different cell impermeable fluorescent dyes (calcein and FITC-dextran). In pulse-chase experiments, the newly formed shell mineral is labelled during the chase, showing that the sea water vacuoles are involved in shell mineralization. Many of these seminal studies were carried out on *A. lobifera* specimens that were re-mineralizing after their shells were partially dissolved using EDTA. This was done in order to be able to visualize the biomineralization process directly using light and confocal microscopy without the interference of the thick shell (Bentov et al., 2009). By contrast, the present study focuses on the Ca^{2+} and Mg^{2+} ion interplay during mineralization in intact *A. lobifera* specimens.

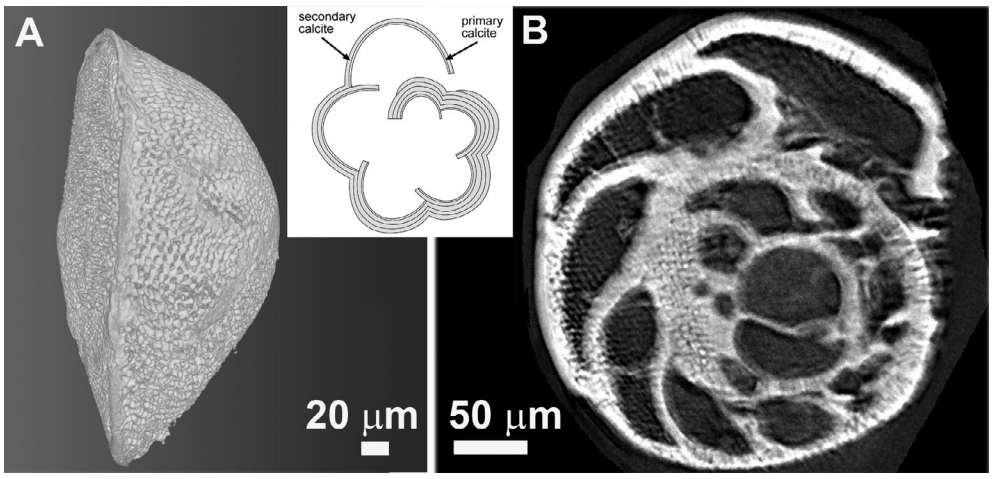

Fig. 1. micro-CT of an *Amphistegina lobifera* shell. (A) 3D reconstruction, lateral view; (B) ventral view of the shell in a semi-horizontal cross-section showing the chambers successively built from the first smaller internal chambers to the most recent larger external chambers. Insert: schematic representation of the lamination process, whereby a new shell layer is added to the entire outer surface with the building of each new chamber (scheme taken from Erez (2003)).

2. Results

The following section shows the development of the correlative cryo-fluorescence–SEM–EDS technique, together with its application in the elucidation of the biomineralization pathways in foraminifera. We present in some detail the results of the method development because we think that it should be widely applicable to mineralized tissues.

2.1. Correlative cryo-SEM/fluorescence microscopy

For the correlative imaging, live specimens of the foraminifera *A. lobifera* and *A. lessoni,* were cultured in calcein-containing sea water for 1–2 days, in order to label the seawater vacuoles and the shells (Bentov et al., 2009). The specimens were then prepared for cryo-SEM imaging by high pressure freezing and freeze fracture. Cryo-SEM is extremely sensitive to surface contamination of ice from residual humidity, so specimens were examined in the SEM first, before fluorescence imaging. Each foraminifer exposed in the fracture was first imaged in cryo-SEM at low magnification (x100–300) in the secondary electron (SE) (Fig. 2A) and backscattered electron (BSE) imaging modes to obtain an overview image of the fracture surface, and its location was documented for future alignment with cryo-fluorescence images. The foraminifer was then systematically scanned in SE and BSE modes (Fig. 2B) and images were taken at medium magnification to cover the entire fracture surface area with an overlap of ~30% between adjacent images. These images were stitched together using Adobe Photoshop to provide a detailed view of the cytoplasm contents. Specific areas of interest were further imaged at higher magnification (Fig. 3A, B, D and E).

The vitrified specimens were then removed from the SEM and transferred in liquid nitrogen into a cryo-Correlative Light Electron Microscopy (cryo-CLEM) stage, pre-cooled to liquid nitrogen temperature. The cryo stage was mounted on an upright confocal laser scanning microscope. Confocal fluorescence images (excitation 488 nm) were acquired simultaneously in red and green channels. Due to the complex topography of the fracture surface it was necessary to collect a stack of images with an extended height range of as much as 100 μm. In each slice the confocal microscope provides optical sectioning from a limited depth of about 2–3 μm, so a simple maximum intensity projection provides an extended depth of field in a single image. This projection was used for alignment to the SEM images.

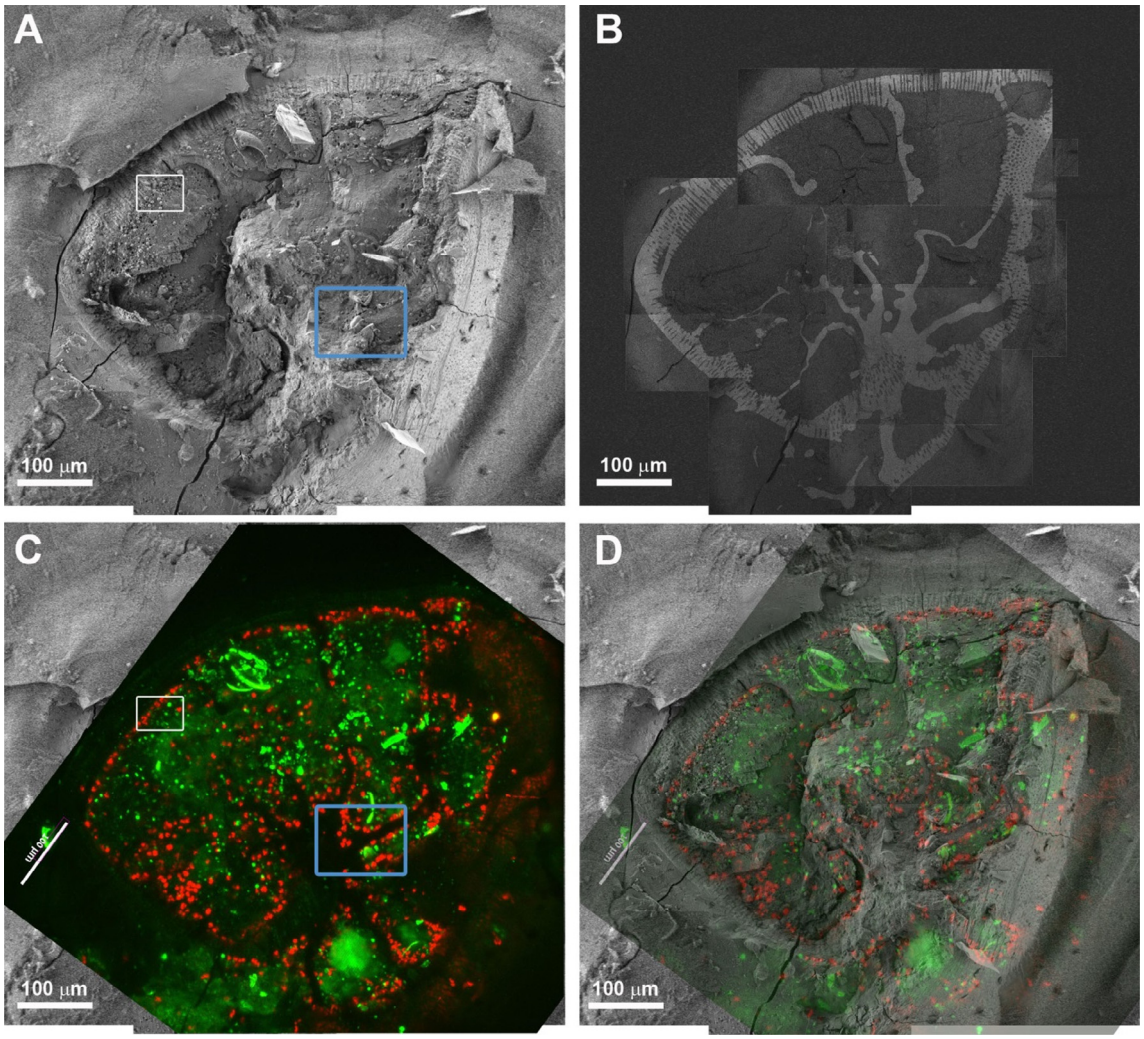

Fig. 2. Correlative cryo-SEM/fluorescence microscopy. (A) Low magnification cryo-SEM image in SE mode of an *A. lessoni* foraminifer after high pressure freezing and freeze-fracture; (B) The same specimen imaged in BSE mode. The shell mineral is seen with high contrast. The micrograph was obtained by stitching together tens of higher magnification images that were taken with partial overlap to facilitate reconstruction. (C) Fluorescence image of the same specimen. Symbionts are red and calcein staining is green. (D) Overlay of the fluorescence image on the electron microscope SE image. The shell and the symbionts are used for alignment. White and blue rectangles in A and C designate the areas examined at higher magnification in Fig. 3.

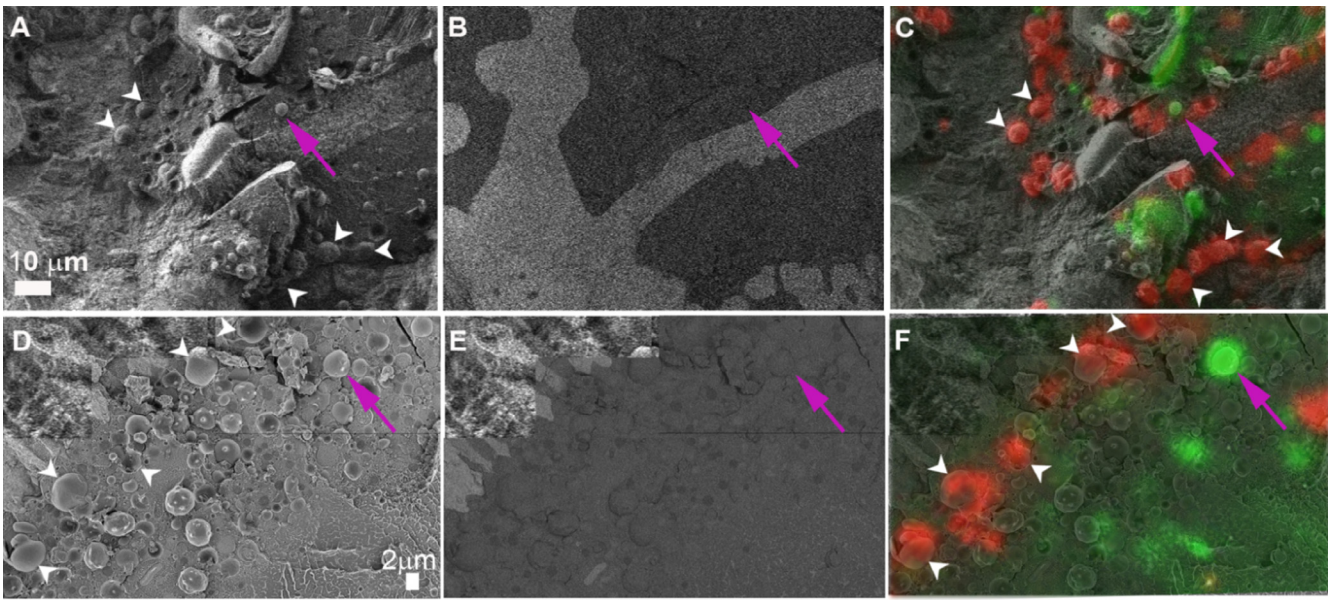

Fig. 3. Correlative cryo-SEM/fluorescence microscopy, *A. lessoni*. A–C: Medium magnification micrographs of the region delimited by the blue square in Fig. 2. (A) SE mode: part of the shell and many organelles are visible, several of which are recognizable as symbionts because of their typical morphology (white arrowheads); (B) BSE mode: only the shell shows higher contrast, whereas none of the organelles are distinguishable. (C) Fluorescence image overlaid on the SE micrograph. Red: symbiont auto-fluorescence; green: calcein labeling. D–F: Higher magnification micrographs of the region delimited by the white square in Fig 2. (D) SE mode; (E) BSE mode; (F) Fluorescence image overlaid on the SE micrograph. The red symbiont anchors (white arrowheads) serve to accurately re-align the images in successive cycles at higher magnification. The magenta arrows identify vesicles that are clearly visible in (A) and (D), are strongly fluorescent (green) in (C) and (F), but have no signal in (B) and (E), indicative of low calcium concentrations.

Alignment of the fluorescence and SEM images required several refinement steps. The projected fluorescence images of the foraminifer fracture surface were first manually overlaid onto the low magnification SE SEM micrographs. Preliminary alignment was based on the outlines of the shell (external walls and internal chambers). The fluorescence image was resized to the size of the SE SEM micrograph of medium magnification containing the fracture surface collage (according to the magnification ratio between the low magnification and medium magnification SE micrographs). Adjustments to the alignment were then made using the shell outline from the backscattered mode collage and the intracellular symbionts as anchors in the SE mode collage and the fluorescence image (Fig. 2C and D). Symbionts are characteristically found adjacent to the shell walls.

The symbionts are easily identified by their morphology in the SE micrographs and by their red auto-fluorescence. However, the fluorescence originates from an optical section that extends below the fracture surface by as much as 2–3 µm, whereas the secondary electrons are emitted from only tens of nm beneath the surface. Therefore many of the fluorescent objects do not correspond to a fractured symbiont in the SEM image. Fractured symbionts seen in SEM did, on the other hand, reliably correspond to red fluorescence. A local registration was required to overcome distortions between stitched SEM images and projected confocal fluorescence images. Again symbionts and shell walls were used as registration anchors in each field of view (Fig. 3), but the expectation for global alignment across the entire field was relaxed. Only well aligned images were considered for correlative cryo-SEM/EDS analysis. All image alignments were performed in Adobe Photoshop.

2.2. Vesicles and vacuoles

We observed sea water occlusions in sizes varying from 1 µm or less to tens of microns in the foraminifer cytosol. We distinguish larger endocytosed bodies (tens of micrometers) which exhibit irregular shapes and are referred to here as vacuoles, from small vesicles (few micrometers) which exhibit a round shape and are referred to here as vesicles (Fig. 3A and D). Many of the smaller vesicles are concentrated in the inner chambers, relative to the last formed chamber. In contrast, large calcein labeled sea water occlusions are frequently observed in the recently-formed outer chambers (Fig. 2C and Fig. 4). Cryo-SEM, therefore, confirms that intact foraminifera vacuolize sea water and incorporate it into their cytosol, as was previously demonstrated in partially decalcified foraminifera (Bentov et al., 2009). Many, but not all of these occlusions show labeling with the calcein dye, probably because endo-exocytosis are continuous processes and many seawater vacuoles were produced prior to the labeling period. Note as an example the weak calcein signal from the large vacuole in the center of the image (Fig. 4C and D). The corresponding SE images show that the labelled sea water is occluded inside large membrane-delineated vacuoles (Fig. 4B–D). The sea water vacuoles are better visualized in BSE images (Fig. 4A) because of their characteristic lighter gray color. The higher brightness is due to the high contrast of the dissolved ions present in sea water (chloride in particular), relative to the cytosol, to the other vesicles, and to the symbiont components. Some of the large vacuoles are in contact with the shell surface (Fig. 4A) and may thus provide Ca^{2+} and CO_3^{2-} for building the wall structure.

The hundreds of small uniformly sized (2–3 µm) vesicles with increased calcein signal observed within internal chambers of the shell are substantially different from the sea water vesicles. Note that the absence of the smaller vesicles in the outer chamber could be due to the organism retracting the cytoplasm during handling and/or freezing.

When observed in cryo-SEM, the foraminifer cytoplasm contains many close packed vesicles and cellular organelles (Figs. 2C and 3A, C). The BSE signal of these vesicles is extremely weak relative to the shell wall (Fig. 3B and E) and also relative to the sea water vacuoles, indicating that they do not contain solid calcium-containing mineral deposits, even though their calcein fluorescence signal is intense (Fig. 3C and F).

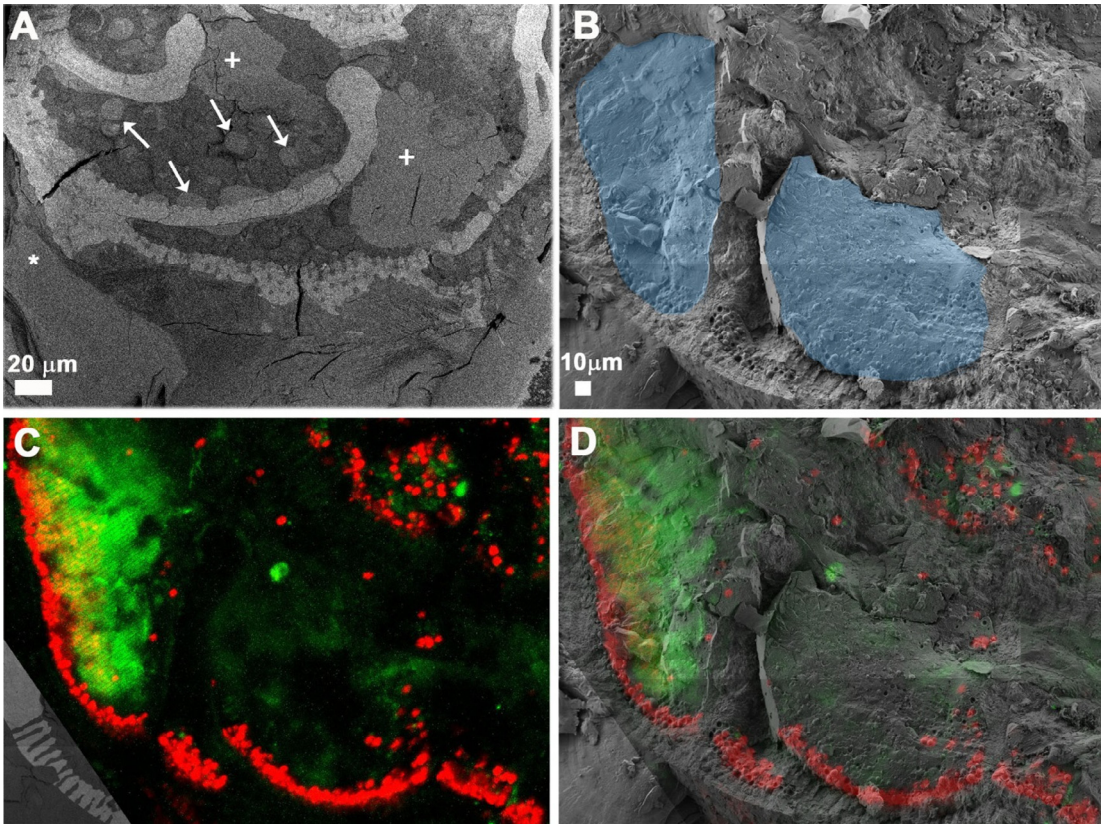

Fig. 4. *A. lobifera*, sea water vacuoles. (A) BSE electron micrograph of a fractured shell, showing larger (crosses) and smaller (arrows) sea water-containing vacuoles. The contrast is due to the high concentration of Na^+ and Cl^-, and is identical to that of external sea water (asterisk). Some of the vacuoles are juxtaposed to the shell wall. B–D: large vacuoles in a different specimen. (B) SE micrograph: two large vacuoles inside the shell have been shaded in light blue for clarity. (C) Fluorescence image, and (D) overlay of fluorescence to SE images: the left vacuole is strongly labeled by calcein, whereas the more internal vacuole is weakly labeled, indicating that it may have been produced mostly prior to the calcein labeling. The apparent lack of homogeneity of calcein labeling in the left vacuole is due to non-labeled inter-chamber compartment walls crossing the vacuole. The cross sections of the compartment walls are visible in B.

2.3. Mg-rich particles

In contrast to the vesicles with spherical morphology and the vacuoles with irregular morphology, we also observed distinct material with irregular shapes. These materials are clearly detected with the BSE detector and are presumably in a solid phase. Some of these dense materials are found in the sea water vacuoles, and some in the cytoplasm. Fig. 5 shows the distribution of a few of these dense particles in a correlative cryo-SEM (SE, BSE)/fluorescence mode. The particles have an increased BSE signal (Fig. 5C), and exhibit a weak, but detectable calcein label in cryo-fluorescence (Fig. 5D). All these particles are found in vesicles and appear to organize around core sheets composed of low electron density material (Fig. 5B).

Using cryo-EDS, we were surprised to discover that the main cation in these dense particles is not calcium, but magnesium. The same frame shown in Fig. 5 is imaged in Fig. 6 by EDS, showing maps for calcium, magnesium, sodium and oxygen. Sodium and oxygen are distributed almost homogeneously (Fig. 6C and D), whereas calcium co-localizes with the shell walls and to some extent with the particles (Fig. 6A). Magnesium clearly co-localizes with the particles detected by BSE imaging and only slightly with the cell walls (Fig. 6B). The low calcein signal detected at the same locations is probably due to the low affinity of calcein for Mg, and/or to small amounts of Ca that are also present in these particles. The Mg-rich particles that do not show calcein labeling may have formed prior to the calcein labeling pulse.

3. Discussion

We have developed a novel correlative imaging and analysis technique that integrates ultrastructural imaging with elemental analysis. The technique combines optical cryo–fluorescence imaging with high resolution morphological, spectroscopic and electron density characterization in the scanning electron microscope. Using this correlative approach, we studied the foraminifer cell cytoplasm under close to physiological conditions, without dissolution of the shell, and analyzed the elemental compositions of different phases within their cellular context. Imaging the interior of shelled organisms is difficult by traditional light microscopy due to scattering by the shell itself. The new method provides a high resolution view of the cytoplasm, symbionts, and various vacuoles and vesicles where ions may be concentrated or removed. The fluorescent dye calcein was used to identify recently endocytosed seawater vacuoles and EDS mapping was used to identify the ions in the BSE dense components. This technique may well have widespread applications to many other shelled single-cell mineralized organisms in addition to foraminifera, such as coccolithophorids, diatoms, radiolaria, ciliates and acantharia etc., as well as for documenting aspects of mineral transport pathways in multicellular organisms.

We confirm the presence of large sea water vacuoles and small vesicles endocytosed into the cytosol. Our observations were made in the natural intact *A. lobifera* specimens and are consistent with earlier observations (Bentov et al., 2009). Within a few hours after

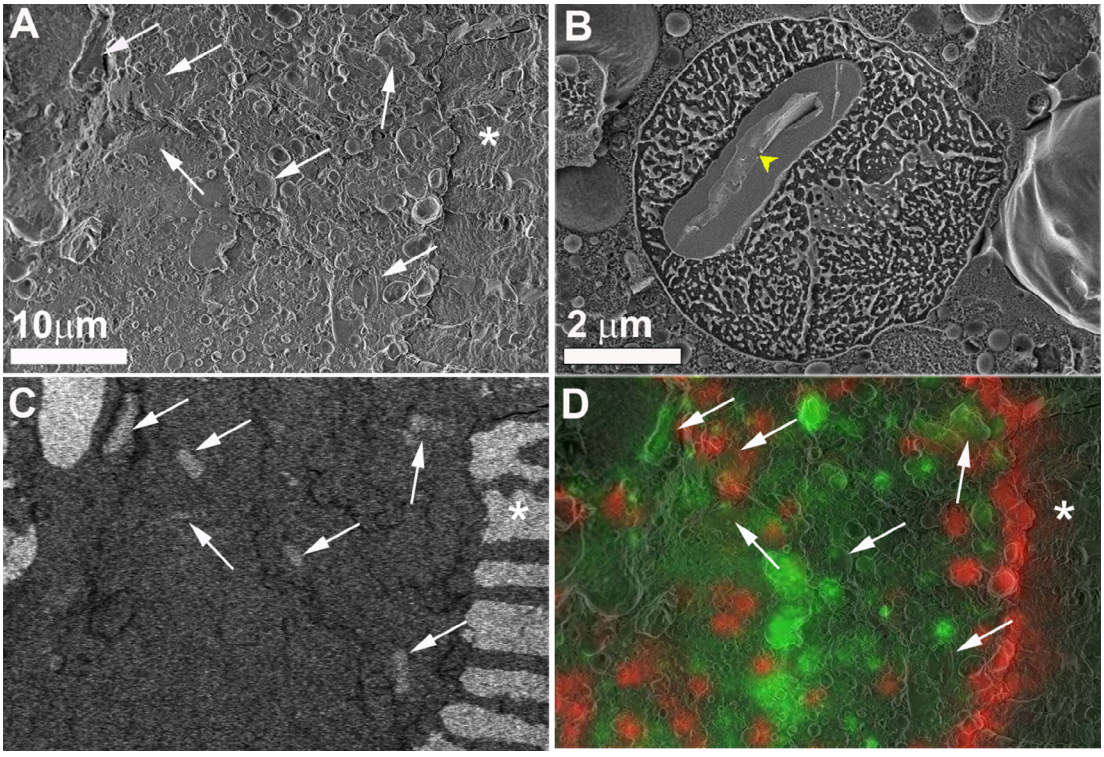

Fig. 5. Mg-rich particles in a specimen of *A. lobifera* (see Mg map in Fig. 6B). Correlative microscopy: (A) SE micrograph, (C) BSE micrograph and (D) overlay of fluorescence on SE micrograph. The shell is marked by an asterisc, and the white arrows mark the position of the Mg rich particles. The Mg rich particles found in the cytoplasm, are electron dense, but are only weakly fluorescent. (B) High magnification of one particle similar to those in A, but imaged from a different specimen; all the magnesium rich particles are found in vesicles and appear to organize around core sheets (arrowhead) composed of low electron density material.

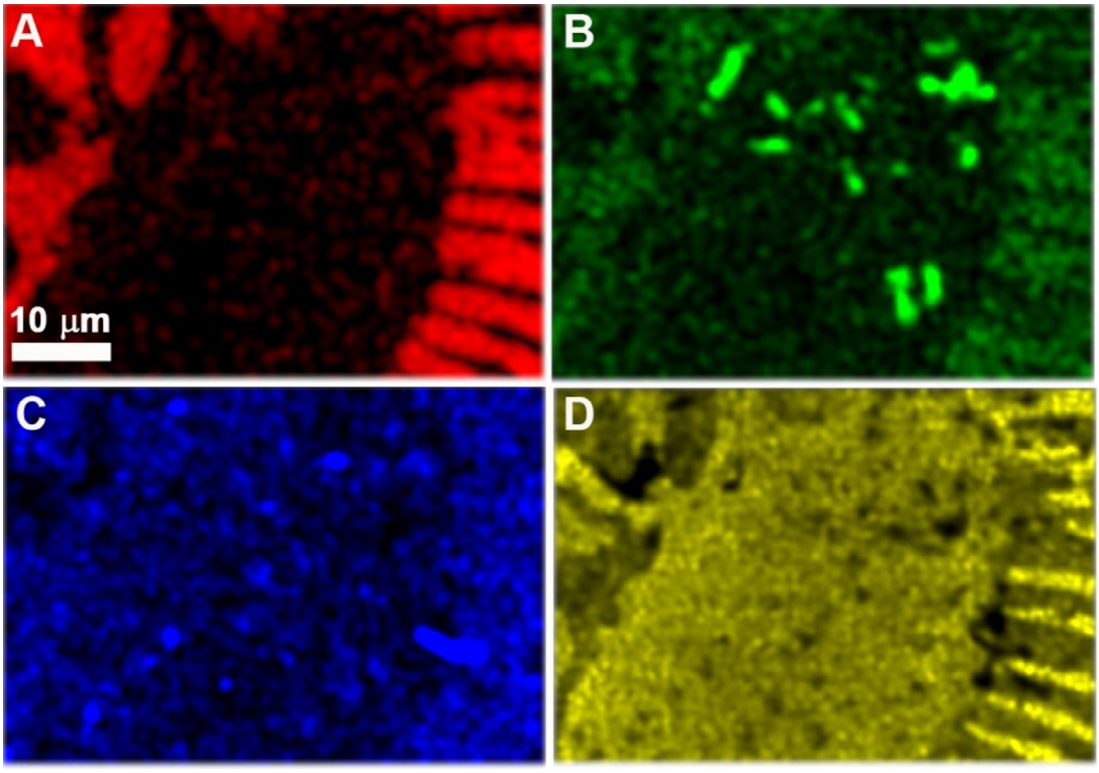

Fig. 6. Cryo EDS mapping of the same frames as in Fig. 5 A, C, D. (A) Calcium map: the shell is clearly evident, but the particles are barely visible; (B) Magnesium map: the shell is barely visible, whereas the signal from the particles is very strong; (C) Sodium map: the signal is uniformly low, with some regions with higher signal that do not correspond to the particles; (D) Oxygen map: the signal is strong over the whole region, and stronger in correspondence to the shell, which is composed of $CaCO_3$.

calcein labelling, we observed in addition to large seawater vacuoles numerous small, rounded and uniformly sized (2–3 μm) fluorescent seawater vesicles. These vesicles have a strong calcein signal (higher than the calcein labeled sea water). They are abundant (hundreds in the fracture surface alone) and can have a life time of a few days in the cytoplasm. The ion concentrations in these vesicles have yet to be determined. They could conceivably be the pool, or one of the pools for calcium storage in the cytoplasm described before (Erez, 2003). They could also be the acidic seawater vesicles described by Bentov et al. (2009).

Of particular note is the presence of high Mg^{2+}-low Ca^{2+} solid particles both in the cytoplasm and in the sea water vacuoles. We indirectly infer that these Mg^{2+}-rich phases may be carbonate mineral particles (absence of phosphorus) that are, or have been during their initial state, in an amorphous phase (no well-defined crystal facets). This needs to be examined directly. Intracellular Mg^{2+}-rich particles engulfed in vacuoles were previously observed in live protoplasmic amoeboids obtained from *A. lobifera* (Bentov and Erez, 2005). These particles are composed of P-Mg^{2+}–Ca^{2+} in a ratio of 3:2:1 and were birefringent, hence crystalline. They were referred to as 'polarizing granules'. We do not know whether the Mg^{2+}-rich particles we observed in this study of intact individuals are the same as those observed in the amoeboids, as they do not contain P or large amounts of Ca.

To our knowledge this is the first time that such a Mg-rich biogenic mineral phase has been reported. As sea water contains about 4–5 times more Mg than Ca, and biogenic calcium carbonates contain much less Mg than Ca, vast amounts of Mg need to be removed from sea water that is used as a source of biogenic calcium (Bentov and Erez, 2006). Furthermore, it is interesting to note that the volume of the sea water mother solution needed to supply enough Mg^{2+} for the mineralization of such micrometer sized Mg-rich particles is at least 200X the volume of the sea water vacuoles within which the particles are observed. This therefore raises the intriguing possibility that the Mg-rich particles are formed in order to remove excess Mg during shell formation. We do know that the sea water vacuoles are removed from the cytoplasm and excreted back into the sea water (unpublished observation by JE).

The challenge of sequestering Mg^{2+} from sea water to lower the Mg:Ca ratio in favor of calcite deposition must be faced by all calcite depositing marine organisms. However, the manner in which different organisms face this challenge is not necessarily the same. The coccolithophorids and sea urchins transfer Ca^{2+} ions from the sea water through selective ion channels that discriminate strongly against Mg^{2+} (Hwang and Lennarz, 1993; Mackinder et al., 2010; Pinsino et al., 2011). The use of incorporated sea water vesicles as a Ca^{2+} reservoir for calcite deposition makes this challenge even more pronounced in foraminifera (Bentov and Erez, 2006).

4. Conclusions

We report here a novel cryo-SEM, cryo-fluorescence and cryo-EDS correlative imaging method that can provide new information on biomineralization pathways of both Ca^{2+} and Mg^{2+} ions from the sea water to the final site of mineral formation. This should be applicable to the study of many biomineralizing organisms. We apply this technique to the study of intact benthic foraminifera, and report the presence of small sea water vesicles in the cytoplasm that label strongly with calcein. We also demonstrate the presence of Mg^{2+}-rich dense mineral particles both in the cytosol and in the sea water vacuoles. We suggest the Mg^{2+}-rich particles may be related to the mechanism of removal of excess Mg^{2+} from sea water. These results support previous reports on the role of seawater vacuolization in the calcification process and contribute to our understanding of shell formation in foraminifera. They raise interesting questions about the Mg^{2+} pathway, about which we know very little in foraminifera, or for that matter in any other organism.

5. Material and methods

5.1. Samples

Specimens of benthic, symbiont-bearing species *A. lobifera* and *A. lessoni* were collected from the Gulf of Eilat, Red Sea, from a depth of 2–6 m. Adult individuals, 0.5–1 mm in size, were cultured in the lab in natural sea water from the Red Sea. Water was changed once every two weeks. Juveniles were obtained from spontaneous asexual reproduction events occurring in the lab.

5.2. Micro-CT

The foraminifer specimen was mounted inside a plastic pipette tip covered with water and was placed in a microCT (MICRO XCT-400, XRadia). Tomography was carried out by using source parameters of 40 kV and 200 mA; 800 images were taken with 15 s exposure time. Raw data were reconstructed with the XRadia software that uses a filtered back-projection algorithm. 3D surface rendering and measurements were carried out with Avizo software (VSG)

5.3. Calcein in vivo labeling

Foraminifera were incubated in freshly made filtered (0.2 μm) seawater solution with 10 μM calcein (Sigma–Aldrich), for 1–2 days. Samples were then washed with filtered (0.2 μm) sea water and observed under a fluorescence microscope (Leica M165 FC). Individuals that had built a new chamber during the pulse period, in which the mineral walls of the last shell chamber were strongly labeled with calcein, were separated from the others. Individuals that did not build a new chamber during the labeling period were taken for high pressure freezing and further cryo-correlative SEM/fluorescence/EDS analysis. A total time of about 1hr passed between washing the samples from the calcein loaded sea water and high pressure freezing.

5.4. Cryo-Scanning Electron Microscopy (SEM) imaging

Calcein labeled or non-labeled *A. lobifera* were cryo immobilized in filtered (0.2 μm) natural sea water solution containing 10%wt Dextran (Fluka) as a cryo protectant, using a high-pressure freezing device (HPM10; Bal-Tec). Adult foraminifera, 0.5–1 mm in diameter and 0.3–0.45 mm thick, were sandwiched between two metal discs (3-mm diameter, 0.25-mm cavities) in groups of 1–3 individuals. Juvenile foraminifera, 3–30 days old (0.15–0.3 mm in diameter and 0.05–0.15 mm thick), were sandwiched between two metal discs (3 mm diameter, 0.05–0.1-mm cavities) in groups of 5–7 individuals. The frozen samples were kept in liquid nitrogen and transferred in a vacuum cryo-transfer device (VCT 100; Bal-Tec) to a freeze-fracture device (BAF 60; Bal-Tec), where they were freeze-fractured at $-120\,^{\circ}C$, 5×10^{-7} mbar. Samples were observed at $-120\,^{\circ}C$ in an Ultra 55 SEM (Zeiss). Each foraminifer was first imaged at low magnification (x100–300) in the secondary electron (SE) mode to obtain an overview image of the fracture surface, and its location in the metal disc (distance from the edges) was documented for future alignment with cryo-fluorescence images. The foraminifer was then systematically scanned and images were taken at medium magnification (2000–10,000X) to cover the entire fracture surface area (up to 1 mm^2) with an overlap of 30% between adjacent images. Specific areas of interest were further imaged at higher magnification. Fracture surfaces of adult

foraminifera were scanned at 2000X magnification using an Everhart–Thornley secondary electron (SE) detector and an in-the-column energy selective backscattered electron (BSE) detector (1 kV, WD = 5 mm). Fracture surfaces of juvenile foraminifera were imaged at 5000–10,000X magnifications using an in-the-column SE detector and an in-the-column BSE detector (1 kV, WD = 2 mm). Images were manually overlaid to form a collage of the entire fracture surface using Adobe Photoshop.

Fractured samples were transferred from the SEM under cryogenic temperature in a vacuum cryo-transfer device (VCT 100; Leica Microsystems). The cryo-transfer device was vented with cold gaseous nitrogen in the freeze-fracture device (BAF 060; Bal-Tec). Samples were unloaded into liquid nitrogen and kept for further cryo-fluorescence and cryo-SEM/EDS analysis.

5.5. Cryo-fluorescence imaging

Vitrified freeze fractured foraminifera samples that were pre-imaged in cryo–SEM were transferred in liquid nitrogen into a cryo-Correlative Light Electron Microscopy (cryo-CLEM) stage (Linkam, model CMS196), pre-cooled to liquid nitrogen temperature. The metal disc containing the sample was mounted on the cooled cryo stage holder, placed a few mm above a liquid nitrogen pool and in the gaseous nitrogen phase. The sample was washed with liquid nitrogen to mechanically remove ice crystals that may have deposited on the sample surface during the transferring procedures. The Linkam cryo stage was mounted on an upright Olympus Fluoview 300 confocal laser scanning microscope. Foraminifera were located on the vitrified sample. After identification of the foraminifer sample, correlative fluorescence data (red and green channels) were collected using Olympus air objective lenses x20/0.45 NA or x40/0.6 NA at a working distance of 3–4 mm. Excitation: 488 nm, dual channel acquisition: 500–530 nm band pass 585 nm long pass and 570 nm beam splitter. The Z stack vertical range was chosen to cover the entire topographic range of the foraminifer fractured surface (about 100 μm) with a step size of 1–1.5 μm. Samples were then transferred back to storage in liquid nitrogen for further cryo-SEM/EDS analysis, when necessary.

5.6. Cryo SEM/energy dispersive X-ray spectroscopy (EDS) analysis

Foraminifera samples were high-pressure frozen, freeze-fractured and cryo-transferred as described above to cryo-SEM imaging in the Ultra plus HR-SEM (Zeiss). Samples were imaged at −120 °C in SE mode and backscattered mode (1 kV, WD = 5 mm). Loci of interest underwent cryo-EDS analysis in the microscope with a working distance of 8 mm and an acceleration voltage of 9 kV using a Bruker Quantax microanalysis system with an AXS-XFlash® detector. Element distribution maps were obtained using the Quantax software. EDS map brightness and contrast levels were adjusted using Adobe Photoshop.

5.7. Cryo-SEM/fluorescence/EDS analysis

Vitrified foraminifera samples underwent correlative cryo–SEM/fluorescence analysis and loci of interest were documented. Samples were kept pre-fractured, in liquid nitrogen. The pre-fractured vitrified samples were washed with liquid nitrogen to remove possible ice crystals adsorbed to the fracture surface during the transfer procedure. Samples were then loaded from liquid nitrogen to a cryo-transfer device (VCT 100; Bal-Tec) pre-vented with cold gaseous nitrogen. The cryo-transfer device was then pumped to 5×10^{-7} mbar in the freeze fracture device (BAF 60; Bal-Tec) and was used to transfer the samples to the Ultra plus HR-SEM (Zeiss) for correlative cryo-SEM/EDS observation. Samples were scanned by the ET SE detector (1 kV, WD = 5 mm) and loci of interest were re-located. Cryo-EDS mapping at different magnifications was carried out on chosen locations (9 kV, WD = 8 mm) using a Bruker Quantax microanalysis system with an AXS-XFlash® detector. Element distribution maps were obtained using the Quantax software.

Acknowledgements

We thank Shai Oron and the entire InterUniversity Institute (IUI) for Marine Sciences in Eilat for their help with sample collection. We thank Eyal Shimoni, Elena Kartvelishvily and Ofer Dudovitch from the Weizmann Institute of Science Electron Microscopy Unit for their help and support with the cryo-SEM microscopy, and Vlad Brumfeld for support with the microCT. We thank Netta Vidavsky for helping with the manuscript editing. The cryo-EDS work was performed in the Technion Laboratory for Electron Microscopy of Soft Materials, supported by the Technion Russell Berrie Nanotechnology Institute (RBNI). This research was supported by the Israel Science Foundation (Grant # 551/10 to J.E.), a German Research Foundation grant, within the framework of the Deutsch-Israelische Projektkooperation. L.A. is the incumbent of the Dorothy and Patrick Gorman Professorial Chair of Biological Ultrastructure, S.W. is the incumbent of the Dr. Trude Burchardt Professorial Chair of Structural Biology.

Appendix A. Supplementary data

Supplementary data associated with this article can be found, in the online version, at http://dx.doi.org/10.1016/j.jsb.2016.01.015.

References

Anderson, O.R., Faber, W.W., 1984. An estimation of calcium carbonate deposition rate in a planktonic foraminifer *Globigerinoides sacculifer* using ^{45}Ca as a tracer; a recommended procedure for improved accuracy. J. Foraminiferal Res. 14, 303–308.

Angell, R.W., 1979. Calcification during chamber development in *Rosalina floridana*. J. Foraminiferal Res. 9, 341–353.

Bentov, S., Brownlee, C., Erez, J., 2009. The role of seawater endocytosis in the biomineralization process in calcareous foraminifera. Proc. Nat. Acad. Sci. U.S.A. 106, 21500–21504.

Bentov, S., Erez, J., 2005. Novel observations on biomineralization processes in foraminifera and implications for Mg/Ca ratio in the shells. Geology 33, 841–844.

Bentov, S., Erez, J., 2006. Impact of biomineralization processes on the Mg content of foraminiferal shells: a biological perspective. Geochem. Geophys. Geosyst. 7, 1525–1536.

Broecker, W.S., Peng, T.-H., 1982. Tracers in the Sea. Eldigio Press, Palisades, New York.

Cushman, J.A., 1947. Foraminifera. Their Classification and Economic Use. Harvard University Press, Cambridge, MA.

Duenas-Bohorquez, A., Raitzsch, M., de Nooijer, L.J., Reichart, G.-J., 2011. Independent impacts of calcium and carbonate ion concentration on Mg and Sr incorporation in cultured benthic foraminifera. Mar. Micropaleontol. 81, 122–130.

Emiliani, C., 1955. Pleistocene temperatures. J. Geol. 63, 538–578.

Erez, J., 2003. The source of ions for biomineralization in foraminifera and their implications for paleoceanographic proxies. In: Dove, P.M., De Yoreo, J.J., Weiner, S. (Eds.), Biomineralization. Mineralogical Society of America, Washington DC, pp. 115–149.

Hansen, H.J., Reiss, Z., 1971. Electron microscopy of rotaliacean wall structures. Bull. Geol. Soc. Denmark 20, 329–346.

Hemleben, C., Spindler, M., Anderson, O.R., 1989. Modern Planktonic Foramnifera. Springer-Verlag, NY, Berlin, Heidelberg.

Hottinger, L., 1986. Construction, structure, and function of foraminiferal shells. In: Leadbeater, B.S.C., Riding, R. (Eds.), Biomineralization in Lower Plants and Animals. Clarendon press, Oxford.

Hwang, S.P., Lennarz, W.J., 1993. Studies on the cellular pathway involved in assembly of the embryonic sea urchin spicule. Exp. Cell Res. 205, 383–387.

Katz, M.E., Cramer, B.S., Franzese, A., Honisch, B., Miller, K.G., Rosenthal, Y., Wright, J. D., 2010. Traditional and emerging geochemical proxies in foraminifera. J. Foraminiferal Res. 40, 165–192.

Lea, D.W., Martin, P.A., Chan, D.A., Spero, H.J., 1995. Calcium uptake and calcification rate in the planktonic foraminifer *Orbulina universa*. J. Foraminiferal Res. 25, 14–23.

Lee, J.J., Anderson, O.R., 1991. Cytology and fine structure. In: Lee, J.J., Anderson, O.R. (Eds.), Biology of Foraminifera. Academic Press London.
Mackinder, L., Wheeler, G., Schroeder, D., Riebesell, U., Brownlee, C., 2010. Molecular mechanisms underlying calcification in coccolithophores. Geomicrobiol. J. 27, 585–595.
Mewes, A., Langer, G., Thoms, S., Nehrke, G., Reichart, G.J., de Nooijer, L.J., Bijma, J., 2015. Impact of seawater [Ca2+] on the calcification and calcite Mg/Ca of *Amphistegina lessoni*. Biogeosciences 12, 2153–2162.
Murray, J.W., 1991. Ecology and distribution of benthic foraminifera. In: Lee, J.J., Anderson, O.R. (Eds.), Biology of Foraminifera. Academic Press, London, pp. 222–250.
Nehrke, G., Keul, N., Langer, G., de Nooijer, L.J., Bijma, J., Meibom, A., 2013. A new model for biomineralization and trace-element signatures of foraminifera tests. Biogeosciences 10, 9797–9818.
Pinsino, A., Roccheri, M.C., Costa, C., Matranga, V., 2011. Manganese interferes with calcium, perturbs ERK signaling, and produces embryos with no skeleton. Toxicol. Sci. 123, 217–230.
Raitzsch, M., Duenas-Bohorquez, A., Reichart, G.J., de Nooijer, L.J., Bickert, T., 2010. Incorporation of Mg and Sr in calcite of cultured benthic foraminifera: impact of calcium concentration and associated calcite saturation state. Biogeosciences 7, 869–881.
ter Kuile, B., Erez, J., 1987. Uptake of inorganic carbon and internal carbon cycling in symbiont-bearing benthonic foraminifera. Mar. Biol. 94, 499–509.
ter Kuile, B., Erez, J., 1988. The size and function of the internal inorganic carbon pool of the foraminifer *Amphistegina lobifera*. Mar. Biol. 99, 481–487.
ter Kuile, B., Erez, J., Padan, E., 1989. Mechanisms for the uptake of inorganic carbon by two species of symbiont-bearing foraminifera. Mar. Biol. 103, 241–251.
Toyofuku, T., de Nooijer, L.J., Yamamoto, H., Kitazato, H., 2008. Real-time visualization of calcium ion activity in shallow benthic foraminiferal cells using the fluorescent indicator Fluo-3 AM. Geochem. Geophys. Geosyst. 9. http://dx.doi.org/10.1029/2007GC001772.
Wefer, G., Berger, W.H., Bijma, J., Fischer, G., 1999. Clues to ocean history: a brief overview of proxies. In: Fisher, G., Wefer, G. (Eds.), Use of Proxies in Paleoceanography: Examples from the South Atlantic. Springer-Verlag, Berlin and Heidelberg, pp. 1–68.